

Size Control of Mesoscale Aqueous Assemblies of Quantum Dots and Block Copolymers

Huda Yusuf, Whan-Gi Kim,[†] Dong Hoon Lee,[†] Yunyong Guo, and Matthew G. Moffitt*

Department of Chemistry, University of Victoria, P. O. Box 3065, Victoria, British Columbia V8W 3V6, Canada

Received August 9, 2006. In Final Form: October 6, 2006

Dropwise addition of water to blend solutions of block copolymer-stabilized quantum dots (QDs) and amphiphilic block copolymer stabilizing chains PS(665)-*b*-PAA(68) (PS = polystyrene, PAA = poly(acrylic acid)) in DMF induces self-assembly to form photoluminescent mesoscale QD/block copolymer colloids in water termed QD compound micelles (QDCMs). Here we demonstrate reproducible kinetic control of QDCM particle size and chain stretching within the external PAA stabilizing layer via changes in the initial polymer concentration and rate of water addition. By increasing the initial polymer concentration or decreasing the rate of water addition for a constant blend composition, larger QDCM particles are obtained. From a combination of transmission electron microscopy and dynamic light scattering, the thickness of the external PAA layer is determined for various QDCM sizes, showing that PAA stretching in the external brush layer increases with increasing particle size, reaching the limit of fully extended chains for sufficiently large particles. The photoluminescence spectra from QDCMs in pure water indicate that photoluminescence properties of the block copolymer-stabilized QD building blocks are retained during self-assembly. The demonstrated control of mesoscale particle size and conformation of the stabilizing PAA layer, among other related structural parameters, via simple variation of experimental conditions is a promising step toward the application of QDCM assemblies in photonics and biolabeling.

Introduction

Metal and semiconductor nanoparticles offer unique size-tunable properties arising from quantum confinement and surface effects (e.g., photoluminescence, nonlinear optical properties, surface plasmon resonances). With a view to designing complex structures for applications ranging from biolabeling to photonics, a range of recent research efforts have focused on various self-assembly strategies to control the organization of nanoparticle building blocks in colloidal media.^{1–36} In particular, a number

of groups have developed methods of forming nanoparticle/polymer colloids in which mesoscale composite particles are assembled from multiple metal or semiconductor nanoparticles via a polymer component which can act as a scaffold, glue, or matrix.^{12–36} To this end, supramolecular assembly of nanoparticle “bricks” and polymer “mortar”,^{13–19} electrostatic assembly of nanoparticles on preformed polymer spheres,^{20–23} emulsion and suspension polymerization of composite spheres,^{24–27} and swelling and nanoparticle loading of hydrogel spheres^{28,29} have all been demonstrated. Common to all of these strategies is the potential to engineer the properties of hierarchical colloidal architectures for specific applications, by independent tuning of the nature of individual components and their organization on multiple length scales.

A key challenge in the self-assembly of composite nanoparticle/polymer colloids is the simultaneous control over both the nanoparticle spacing^{15,16} within the composite particles and the overall mesoscale particle size.^{7,8,31} Nanoparticle spacing is well-known to influence the optical, electronic, and magnetic properties

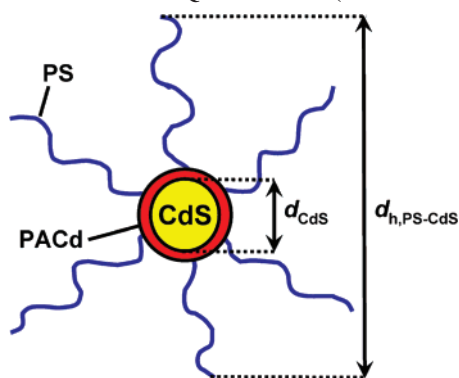
* To whom correspondence should be addressed: E-mail: mmoffitt@uvic.ca.

[†] Present address: Department of Applied Chemistry, Konkuk University, 322 Danwol, Chungju, Chungbuk, Korea 380-220.

- (1) Adachi, E. *Langmuir* **2000**, *16*, 6460.
- (2) Chen, Y.; Rosenzweig, Z. *Nano Lett.* **2002**, *2*, 1299.
- (3) Chen, Y.; Ji, T.; Rosenzweig, Z. *Nano Lett.* **2003**, *3*, 581.
- (4) Yonezawa, T.; Matsune, H.; Kimizuka, N. *Adv. Mater.* **2003**, *15*, 499.
- (5) Faul, C. F. J.; Antonietti, M. *Adv. Mater.* **2003**, *15*, 673.
- (6) Ryadnov, M. G.; Ceyhan, B.; Niemeyer, C. M.; Woolfson, D. N. *J. Am. Chem. Soc.* **2003**, *125*, 9388.
- (7) Maye, M. M.; Luo, J.; Lim, I. S.; Han, L.; Kariuki, N. N.; Rabinovich, D.; Liu, T.; Zhong, C.-J. *J. Am. Chem. Soc.* **2003**, *125*, 9906.
- (8) Maye, M. M.; Lim, I. S.; Luo, J.; Rab, Z.; Rabinovich, D.; Liu, T.; Zhong, C.-J. *J. Am. Chem. Soc.* **2005**, *127*, 1519.
- (9) Stevens, M. M.; Flynn, N. T.; Wang, C.; A., T. D.; Langer, R. *Adv. Mater.* **2004**, *16*, 915.
- (10) Mokari, T.; Serthoock, H.; Aharoni, A.; Ebenstein, Y.; Avnir, D.; Banin, U. *Chem. Mater.* **2005**, *17*, 258.
- (11) Hussain, I.; Wang, Z.; Cooper, A. I.; Brust, M. *Langmuir* **2006**, *22*, 2938.
- (12) Cha, J. N.; Birkedal, H.; Euliss, L. E.; Bartl, M. H.; Wong, M. S.; Deming, T. J.; Stucky, G. D. *J. Am. Chem. Soc.* **2003**, *125*, 8285.
- (13) Shenhar, R.; Norsten, T. B.; Rotello, V. M. *Adv. Mater.* **2005**, *17*, 657.
- (14) Boal, A. K.; Ilhan, F.; E., D. J.; Thurn-Albrecht, T.; Russel, T. P.; Rotello, V. M. *Nature* **2000**, *404*, 746.
- (15) Frankamp, B. L.; Boal, A. K.; Rotello, V. M. *J. Am. Chem. Soc.* **2002**, *124*, 15146.
- (16) Srivastava, S.; Frankamp, B. L.; Rotello, V. M. *Chem. Mater.* **2005**, *17*, 487.
- (17) Maya, L.; Muralidharan, G.; Thundat, T. G.; Kenik, E. A. *Langmuir* **2000**, *16*, 9151.
- (18) Naka, K.; Itoh, H.; Chujo, Y. *Langmuir* **2003**, *19*, 5496.
- (19) Fullam, S.; Rao, S. N.; Fitzmaurice, D. *J. Phys. Chem. B* **2000**, *104*, 6164.
- (20) Caruso, F. *Adv. Mater.* **2001**, *13*, 11.
- (21) Radtchenko, I. L.; Sukhorukov, G. B.; Gaponik, N.; Kornowski, A.; Rogach, A. *Adv. Mater.* **2001**, *13*, 1684.

- (22) Wang, D.; Rogach, A. L.; Caruso, F. *Nano Lett.* **2002**, *2*, 857.
- (23) Hong, X.; Li, J.; Wang, M.; Xu, J.; Guo, W.; Li, J.; Bai, Y.; Li, T. *Chem. Mater.* **2004**, *16*, 4022.
- (24) Sheng, W.; Kim, S.; Lee, J.; Kim, S.-W.; Jensen, K.; Bawendi, M. G. *Langmuir* **2006**, *22*, 3782.
- (25) Joumaa, N.; Lansalot, M.; Theretz, A.; Elaissari, A.; Sukhanova, A.; Artemyev, M.; Nabiev, I.; Cohen, J. H. M. *Langmuir* **2006**, *22*, 1810.
- (26) Sherman, J., R. L.; Ford, W. T. *Langmuir* **2005**, *21*, 5218.
- (27) Yang, X.; Zhang, Y. *Langmuir* **2004**, *20*, 6071.
- (28) Xu, S.; Zhang, J.; Paquet, C.; Lin, Y.; Kumacheva, E. *Adv. Funct. Mater.* **2003**, *13*, 468.
- (29) Kuang, M.; Wang, D.; Bao, H.; Gao, M.; Mohwald, H.; Jiang, M. *Adv. Mater.* **2005**, *17*, 267.
- (30) Moffitt, M.; Vali, H.; Eisenberg, A. *Chem. Mater.* **1998**, *10*, 1021.
- (31) Frankamp, B. L.; Uzun, O.; Ilhan, F.; Boal, A. K.; Rotello, V. M. *J. Am. Chem. Soc.* **2002**, *124*, 892.
- (32) Ma, Y.; Qi, L.; Ma, J.; Cheng, H.; Shen, W. *Langmuir* **2003**, *19*, 9079.
- (33) Duxin, N.; Liu, F.; Vali, H.; Eisenberg, A. *J. Am. Chem. Soc.* **2005**, *127*, 10063.
- (34) Kang, Y.; Erickson, K. J.; Taton, T. A. *J. Am. Chem. Soc.* **2005**, *127*, 13800.
- (35) Kang, Y.; Taton, T. A. *J. Am. Chem. Soc.* **2003**, *125*, 5650.

Scheme 1. Structure of a Block Copolymer-Stabilized Cadmium Sulfide Quantum Dot (PS300–CdS)

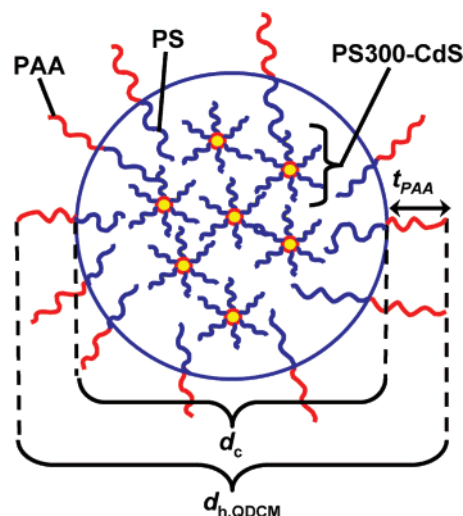


of assemblies.^{13–16} At the same time, the size of nanoparticle/polymer composite particles is critical for biomedical and bioimaging applications, since transport and cell uptake of particles within biological systems are well-known to be size-dependent;^{2,3} for fluorescent imaging applications, particle size will also influence the spatial resolution.² In addition, the size of nanoparticle/polymer assemblies will be an important factor in photonics applications, since mesoscale particle size will determine the wavelength of diffracted light within periodic dielectric structures assembled from these colloids.²⁸

The self-assembly of amphiphilic block copolymers in selective solvents has been shown to provide excellent opportunities for multiscale engineering of nanoparticle/polymer colloids.^{30–36} In 1998,³⁰ Moffitt et al. demonstrated a sequential self-assembly approach to colloidal organization of semiconductor nanoparticles (or quantum dots, QDs): first, self-assembly of a polystyrene-*b*-poly(acrylic acid) (PS-*b*-PAA) copolymer in an organic solvent was induced by addition of cadmium acetate, forming reverse micelles with a poly(cadmium acrylate) (PACd) core; the micelle core was then treated with H₂S to produce a block copolymer-stabilized cadmium sulfide (CdS) QD with an external PS brush (Scheme 1). In a secondary self-assembly step, the PS-coated QDs organized into aqueous quantum dot compound micelles (QDCMs; Scheme 2) upon dropwise addition of water in the presence of additional PS-*b*-PAA stabilizing chains.³⁷ QDCM formation can be explained by phase separation of the PS chains surrounding each QD from the increasingly hydrophilic solvent, with added PS-*b*-PAA chains stabilizing droplets of the polymer-rich phase within an aqueous medium. The complex structural hierarchy of the resulting QDCMs provides a number of attractive features for applications in bioimaging and photonics: (1) Multiple QDs within the hydrophobic QDCM matrix are individually encapsulated inside the hydrophilic cores of self-assembled micelles; QDs are therefore isolated from the external aqueous environment, which should prevent toxic leaching of heavy metal ions during biological applications. (2) The spacing between QDs can be controlled by the degree of polymerization and aggregation number of PS blocks surrounding each QD, independent of the QDCM size. (3) The external PAA brush layer is charged at sufficiently high pH, providing opportunities for electrostatic binding with biological molecules and for control of interparticle interactions and transport properties.

Despite the promise of QDCMs for biological and photonics applications, control over their mesoscale sizes has not been

Scheme 2. Structure of a QDCM



previously reported. In fact, to our knowledge, only two papers have previously demonstrated size control of self-assembled nanoparticle/polymer colloids, one by varying the temperature of supramolecular “bricks and mortar” self-assembly,¹⁴ and the other by varying the concentration of magnetic nanoparticles incorporated into PS-*b*-PAA block copolymer micelles.³⁶ In this paper, we present two new kinetic strategies for controlling the sizes of mesoscale QDCM composite spheres, by varying either the initial polymer concentration or the rate of water addition during self-assembly. Both methods rely on the kinetic nature of QDCM sizes, which depend on a window of growth between the onset of self-assembly at the critical water content (CWC) and the freezing of particle growth above the CWC. In addition, we extend the multiscale engineering of self-assembled hierarchical colloids by demonstrating the first example of systematic control over chain packing and polymer conformation in the stabilizing layer, indicating feasibility of tuning colloidal interactions for biolabeling or self-assembly of photonic structures. Using a combination of dynamic light scattering (DLS) and transmission electron microscopy (TEM) data for various QDCM sizes, we demonstrate that control of PAA packing density allows the chain stretching within the PAA layer to be tuned, with up to 100% stretching suggesting a highly charged stabilizing layer at pH 6. Finally, we investigate the photoluminescence (PL) from these QDCM assemblies, which is found to be qualitatively identical with PL emission from individual block copolymer-stabilized QDs dispersed in dilute solutions. This result indicates that semiconductor QDs can be assembled into these complex and controllable colloids without photoluminescence changes associated with agglomeration, ripening, or changes in refractive index at the QD surface.

Experimental Section

Synthesis of PS-*b*-PAA Diblock Copolymers. Anionic polymerization of PS-*b*-PtBA and subsequent hydrolysis to PS-*b*-PAA was used to synthesize both of the PS-*b*-PAA diblock copolymers used for this study: PS(300)-*b*-PAA(12) (used to prepare the block copolymer-stabilized CdS QDs) and PS(665)-*b*-PAA(68) (used as stabilizing chains during QDCM formation), where numbers in parentheses indicate number-average degrees of polymerization. Details on synthesis and characterization of PS-*b*-PAA diblock copolymers by anionic polymerization and hydrolysis are provided in various references.^{38,39} Following hydrolysis, the copolymers were

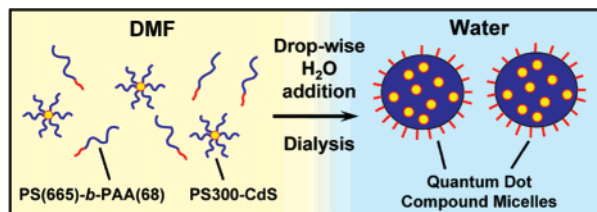
(36) Kim, B.-S.; Qiu, J.-M.; Wang, J.-P.; Taton, T. A. *Nano Lett.* **2005**, *5*, 1987.

(37) QDCMs were labeled “large compound micelles” or “LCMs” in ref 30. Here we use the more appropriate term QDCM to distinguish these QD assemblies from LCM colloids which do not contain QDs (see, for example, refs 46 and 47) which are formed from PS-*b*-PAA copolymers with very small PAA contents.

(38) Desjardins, A.; Eisenberg, A. *Macromolecules* **1991**, *24*, 5779.

(39) Zhong, X. F.; Varshney, S. K.; Eisenberg, A. *Macromolecules* **1992**, *25*, 7160.

Scheme 3. Formation of Quantum Dot Compound Micelles via Self-Assembly of PS300–CdS and PS(665)-*b*-PAA(68) in DMF/Water Mixtures



fractionated using an established procedure,⁴⁰ to remove most of the PS homopolymer impurity present from killing during anionic polymerization. The PS homopolymer content of the final fractionated copolymers was <8 wt %.

Preparation of Block Copolymer-Stabilized CdS Quantum Dots (PS300–CdS). Starting with the diblock copolymer PS(300)-*b*-PAA(12), block copolymer-stabilized quantum dots, such as represented in Scheme 1, were prepared in a process that involves the following steps: (1) micellization of PS-*b*-PAA by the addition of cadmium acetate in organic solvent to form block ionomer reverse micelles containing cadmium ions in the core, (2) templated growth of a single CdS QD within each micelle core, (3) reneutralization of the PAA layer with cadmium acetate to stabilize the hybrid particle. Further experimental details are provided in earlier papers from our group.^{41,42} The final, kinetically locked block copolymer-stabilized QDs were recovered as a yellow powder and designated PS300–CdS, where PS300 refers to the degree of polymerization of PS chains in the external brush layer and CdS refers to the QD in the micelle core.

Preparation of QDCMs. The QDCM assemblies described in this paper were prepared using the following general procedure: PS(665)-*b*-PAA(68), used as stabilizing chains, and PS300–CdS were each dissolved in separate DMF solutions to an initial polymer concentration, C_0 , and both solutions were stirred overnight at room temperature. The DMF used was 99.9+ % HPLC grade, $[H_2O] < 0.03$ wt %; the bottle was sealed with Teflon when not in use. These solutions were then mixed in different ratios to obtain various blend solutions with initial polymer concentration, C_0 , and different compositions designated by the weight fraction of PS300–CdS, f , relative to the total polymer content.

To ~5 g of each blend solution was added deionized water dropwise at a constant rate, $rate_{H_2O}$, with rapid stirring (Scheme 3), noting the point at which an increase in turbidity indicated the onset of QDCM formation at the CWC. Water addition was continued at the same rate up to 25 wt % water, at which point particle sizes are kinetically frozen, irrespective of subsequent changes in water content. The QDCM samples were finally dialyzed against deionized water to remove all DMF for characterization by TEM and DLS.

The various QDCM samples prepared for this work are therefore described by three variables of sample preparation: f , C_0 , and $rate_{H_2O}$. Each series of experiments involved several QDCM preparations with one of these three experimental parameters varied. All experiments in a series were carried out consecutively on the same day. For all preparations, the stirring rate during water addition was held approximately constant by using the same setting on the stir plate with identical stir bars; this did not account for viscosity differences from different initial polymer concentrations, though none of the solutions were too viscous to allow for rapid stirring. The laboratory temperature was monitored over the course of all the experiments (water addition and dialysis) and was found to be 22.5 ± 1 °C.

Static Light Scattering. Static light scattering (SLS) of PS300–CdS in DMF was carried out to characterize the aggregation number, Z , and the radius of gyration, r_g , of the block copolymer-stabilized CdS QDs before secondary self-assembly to form QDCMs. The

SLS experiments were carried out on a Brookhaven Instruments multiangle system equipped with a BI-200SM goniometer and a Melles Griot He–Ne laser (632.8 nm) with maximum power output of 75 mW. SLS measurements were carried out in a concentration range from 1 to 0.1 mg/mL, and the angles of detection ranged from 15° to 155° with 5° increments between measurements. Ten repeat measurements of scattered light intensity were taken at each angle and concentration. The reported aggregation number and radius of gyration were determined for the average results of two separate Zimm plots obtained from different stock solutions. All SLS measurements were conducted at 23 °C.

Dynamic Light Scattering. All DLS experiments were carried out on a Brookhaven Instruments photon correlation spectrometer equipped with a BI-200SM goniometer, a BI-900AT digital autocorrelator, and a Melles Griot He–Ne laser (632.8 nm) with maximum power output of 75 mW. All DLS measurements were conducted at 23 °C.

DLS of PS300–CdS in DMF was carried out to characterize the hydrodynamic diameter, $d_{h,PS-CdS}$, of the block copolymer-stabilized QDs before secondary self-assembly to form QDCMs. The z -average $d_{h,PS-CdS}$ value for PS300–CdS in DMF was determined by analyzing the autocorrelation function using the method of cumulants for a range of scattering angles and a range of concentrations from 1 to 0.10 mg/mL.

DLS measurements of selected dialyzed QDCM samples in deionized water (pH 6) were conducted at a single scattering angle of 90°. All QDCM samples were diluted for DLS measurements to obtain a time-average scattering intensity of ~500 kcps for a constant pinhole size (100 μm), with concentrations varying from 0.1 to 0.01 mg/mL for different particle sizes. To ensure that each measurement gave an apparent particle size that was independent of concentration, the samples run at the highest concentrations according to the above criterion were diluted by a factor of 10 and remeasured, and the apparent particle size did not change significantly. For each experiment, three repeat measurements of the autocorrelation function were obtained.

UV–Vis and Photoluminescence Measurements. Absorption spectra of PS300–CdS were recorded on a Cary 50-scan UV–vis spectrophotometer using samples dissolved in spectroscopic grade toluene with pure spectroscopic grade toluene subtracted as the background. Static PL measurements of PS300–CdS and selected QDCM samples were recorded on an Edinburgh Instruments FLS 920 instrument equipped with a Xe 450 W arc lamp and a red-sensitive PMT (R928-P). All PL spectra were recorded at 1 nm spectral resolution, and the solvent background was subtracted.

Transmission Electron Microscopy. TEM of various aqueous QDCM colloids was performed on a Hitachi H-700 electron microscope, operating at an accelerating voltage of 75 kV. QDCMs in pure water were diluted to a concentration of 0.5 mg/mL, and then a 10 μL drop was deposited on a carbon-coated Formvar 300-mesh copper grid and then shadowed with Pt/Pd wire for imaging. Particle size analysis and statistics were carried out on the shadowed samples, with various regions of the TEM grid randomly sampled and a minimum of 325 and a maximum 541 particles measured and included in each analysis. Also, images were taken of the same solutions without Pt/Pd shadowing to characterize the QDCM internal structure.

TEM of the PS300–CdS nanoparticles before secondary self-assembly was obtained by depositing dilute solutions (5 mg/mL) of PS300–CdS in benzene onto carbon substrates (without Formvar) on a copper TEM grid. The particles were then imaged on an FEI Tecnai scanning transmission electron microscope, operating at an accelerating voltage of 200 kV. This instrument was also used to obtain high-angle annular dark field (HAADF) scanning TEM (STEM) images for characterization of the QDCM internal structure for some samples.

Results and Discussion

Characterization of Block Copolymer-Stabilized CdS Quantum Dots (PS300–CdS) Dispersed in Organic Solvents. The optical properties of PS300–CdS dispersed in toluene were

(40) Shen, H.; Zhang, L.; Eisenberg, A. *J. Phys. Chem. B* **1997**, *24*, 4697.

(41) Wang, C.-W.; Moffitt, M. G. *Langmuir* **2004**, *20*, 11784.

(42) Wang, C.-W.; Moffitt, M. *Chem. Mater.* **2005**, *17*, 3871.

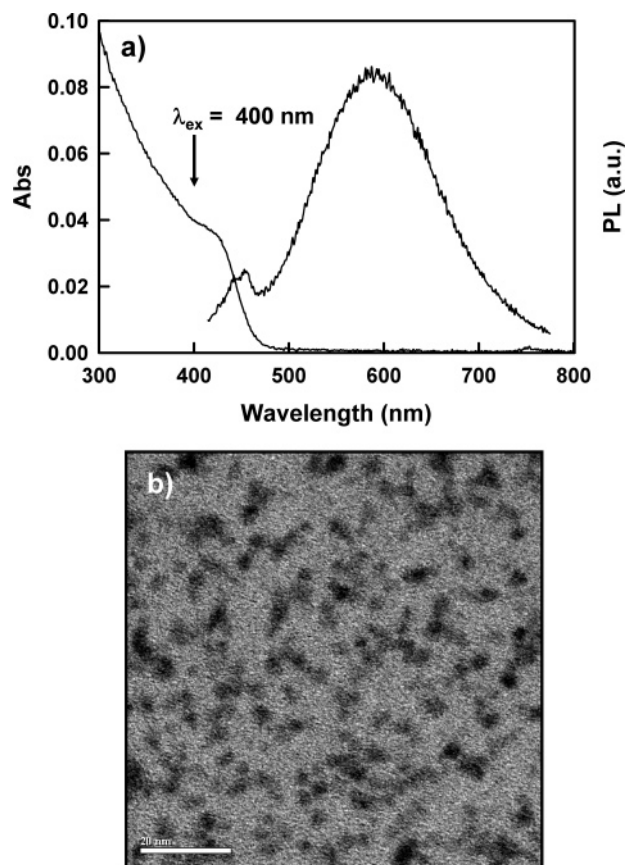


Figure 1. (a) Absorbance and PL spectra of PS300–CdS dissolved in spectroscopic grade toluene ($\lambda_{\text{ex}} = 400$ nm). (b) TEM image of PS300–CdS nanoparticles cast from benzene. The scale bar represents 20 nm.

characterized using UV–vis absorption and PL spectroscopy as shown in Figure 1a. The UV–vis absorption spectrum shows an exciton shoulder at ~ 430 nm with an absorption threshold of $\lambda_{\text{thresh}} = 465$ nm, from which the mean CdS QD diameter was calculated to be $d_{\text{CdS}} = 4.0$ nm using the following empirical formula (obtained by fitting data published previously by Henglein): $d_{\text{CdS}} = 1/(0.1338 - 0.0002345\lambda_{\text{thresh}})$.^{43,44} The PL spectrum in Figure 1a was obtained using an excitation wavelength of $\lambda_{\text{ex}} = 400$ nm; the resulting emission shows a broad red-shifted band centered near 600 nm, which is attributed to recombination from a distribution of deep trap states localized at the QD surface. A very weak band-edge emission centered near 450 nm is also visible, which is attributed to recombination from band-edge or near-band-edge states.⁴¹ Figure 1b shows a TEM image of individual PS300–CdS nanoparticles deposited onto a carbon substrate from a dilute benzene solution. Each of the electron-dense dark spots represents the QD core of a single PS300–CdS nanoparticle. Although some particle agglomeration occurs during solution casting, from the TEM image the average diameter of the CdS QDs can be estimated to be ~ 3 nm, in reasonable agreement with the size determined from the UV–vis spectrum. The somewhat larger size determined from λ_{thresh} of the UV–vis spectrum can be understood in terms of a distribution of particle sizes, with the higher wavelength region of the absorption spectrum reflecting larger particles within the distribution.

A general schematic of the structure of block copolymer-stabilized QDs dispersed in organic solvents is presented in

Table 1. Structural Characteristics of PS300–CdS in DMF (SLS and DLS Data)

M_w	z	r_g (nm)	$d_{h,\text{PS-CdS}}$ (nm)	r_g/r_h	d_{CdS} (nm)
$(1.78 \pm 0.06) \times 10^6$	54 ± 2	21 ± 8	36 ± 2	1.2 ± 0.4	4.0

Scheme 1, with specific structural characteristics determined for PS300–CdS dispersed in DMF solutions summarized in Table 1. From SLS, the weight-average molecular weight of PS300–CdS is $M_w = 1.78 \pm 0.06 \times 10^6$, from which an aggregation number of $Z = 54 \pm 2$ PS(300)-*b*-PACd(12) chains surrounding each CdS QD was determined. Also from SLS, the radius of gyration, r_g , of PS300–CdS in DMF was determined to be 21 ± 8 nm. Dynamic light scattering was used to determine the hydrodynamic diameter of PS300–CdS in DMF, $d_{h,\text{PS-CdS}} = 36 \pm 2$. The ratio r_g/r_h from a combination of SLS and DLS results is known to provide structural information on particles in solution, with $r_g/r_h = 0.775$ indicating hard spheres and $r_g/r_h \approx 1.1$ being found for spherical starlike particles.⁴⁵ Using the hydrodynamic radius $r_{h,\text{PS-CdS}} = 18 \pm 1$ nm determined from DLS and the radius of gyration $r_g = 21 \pm 8$ nm determined from SLS, we obtain a ratio $r_g/r_h \approx 1.2 \pm 0.4$ for PS300–CdS dispersed in DMF, which is consistent with well-dispersed, nonaggregated starlike particles.

Overview of QDCM Formation and Kinetic Size Control.

The formation of QDCMs described in this work has certain similarities to the self-assembly of PS-*b*-PAA crew-cut micelles described extensively in the literature,^{40,46–51} along with important differences. Before the present strategy of kinetic size control of QDCMs is described, therefore, a brief overview of the relative roles of thermodynamics and kinetics in the formation PS-*b*-PAA crew-cut micelles will be given.

A common method of crew-cut micelle formation begins with the dissolution of single chains of PS-*b*-PAA in an organic solvent that is thermodynamically “good” for both blocks and miscible with water (e.g., DMF, THF, dioxane).^{46–50} Water is then added dropwise to the solution, resulting in a progressively poorer solvent for the hydrophobic PS blocks. At the CWC, the PS blocks undergo *microphase separation*, forming a micelle core surrounded by a corona of water-soluble PAA blocks. Above the CWC, the equilibrium size and morphology of the resulting crew-cut micelles will be determined by a free energy minimum, attributed to a balance between the interfacial tension between the core and the solvent and the entropic penalty arising from the stretching of PS chains, which must extend from the interface to the center of the core to maintain constant density.⁴⁷ An increase in water content above the CWC will result in less favorable PS–solvent interactions, effecting a shift in equilibrium toward increasing micelle aggregation numbers, along with morphological transitions from spheres to rods and then from rods to vesicles.⁴⁹ Along with this thermodynamic effect of water addition, increasing water content will also slow the kinetics of structural reorganization. Just above the CWC, the micelles exist in dynamic equilibrium with single copolymer chains due to the plasticization of the cores with organic solvent: the micelles can therefore rapidly rearrange in response to a shift in equilibrium (e.g., induced by water addition).⁴⁹ However, with continued water addition, the organic solvent is progressively leached out

(45) Burchard, W. *Adv. Polym. Sci.* **1983**, *48*, 1.

(46) Zhang, L.; Eisenberg, A. *Science* **1995**, *268*, 1728.

(47) Zhang, L.; Eisenberg, A. *J. Am. Chem. Soc.* **1996**, *118*, 3168.

(48) Zhang, L.; Shen, H.; Eisenberg, A. *Macromolecules* **1997**, *30*, 1001.

(49) Zhang, L.; Eisenberg, A. *Macromolecules* **1999**, *32*, 2239.

(50) Zhang, L.; Eisenberg, A. *J. Polym. Sci., Part B: Polym. Phys.* **1999**, *37*, 1469.

(51) Zhang, L.; Barlow, R. J.; Eisenberg, A. *Macromolecules* **1995**, *28*, 6055.

(43) Henglein, A. *Chem. Rev.* **1989**, *89*, 1861.

(44) Moffitt, M.; McMahon, L.; Pessel, V.; Eisenberg, A. *Chem. Mater.* **1995**, *7*, 1185.

of the cores, decreasing the mobility of PS chains; above a certain water content (between 8 and 11 wt % water), the micelles become kinetically frozen on the time scale of further water addition.^{48–50} Following dialysis, the resulting aggregate morphologies in pure water are therefore not equilibrium structures, although they can be regarded as “snapshots” of earlier thermodynamic states.

Similar to crew-cut micelle formation, the formation of QDCMs described here begins with the dropwise addition of water to a polymer solution in DMF, although in this case two components are present: amphiphilic PS-*b*-PAA stabilizing chains and hydrophobic PS300–CdS particles (Scheme 3). Just as in crew-cut micelle formation, a CWC exists above which PS chains undergo phase separation from the DMF/water mixture. Since the PS300–CdS is the higher molecular weight component, it will phase separate first,⁴⁸ defining the CWC of the mixture. Unlike the formation of crew-cut micelles, this is a *macrophase separation* process,^{48,52–54} with the hydrophobic PS300–CdS particles forming a polymer-rich phase within a solvent phase via spinodal decomposition, eventually breaking into spherical clusters of PS300–CdS particles. Upon phase separation of PS300–CdS from solution, the PS-*b*-PAA chains will distribute themselves at the interface of the polymer-rich phase and the solvent mixture, lowering the interfacial free energy and slowing particle growth. However, for any water content above the CWC, growth of the spherical clusters and the resulting decrease in surface area will continue to be thermodynamically favorable: the PS blocks of the stabilizing chains are not forced to extend to the center of the hydrophobic phase, so phase coarsening is not restricted by an entropic penalty of PS chain stretching. Therefore, unlike crew-cut micelle formation, an equilibrium QDCM particle size will not exist for any water content, with interfacial tension driving continued QDCM growth above the CWC.

To realize a strategy for QDCM size control, therefore, one must consider the important contribution of kinetics to QDCM growth above the CWC. As water is added dropwise above the CWC, the thermodynamic driving force for phase separation and QDCM growth is increased as the DMF/water mixture becomes progressively poorer for PS. However, at the same time, DMF is progressively forced from the polymer-rich phase as more water is added, decreasing plasticization and lowering the mobility of the polymer chains, similar to the slowing of crew-cut micelle dynamics as the water content is increased. Therefore, at some stage of water addition (expected to be between 8 and 11 wt % water on the basis of previous crew-cut micelle studies),^{48–50} QDCM growth becomes frozen, and QDCMs become locked into an average size that is determined entirely by kinetics. The role of the stabilizing chains is to slow the process of phase separation and QDCM growth to a time scale in which continued water addition can be used to “freeze in” a stable QDCM colloid, as opposed to the fast precipitation of agglomerated PS300–CdS which would otherwise occur.³⁰ We can therefore describe QDCM formation and growth as occurring in a window of time during steady water addition between the CWC and the water content at which QDCMs become effectively frozen. Thus, the average sizes of QDCMs will be influenced by experimental variables that influence the width of this kinetic window. Of these variables, the polymer concentration and the rate of water addition will be investigated here as experimental handles on QDCM size control.

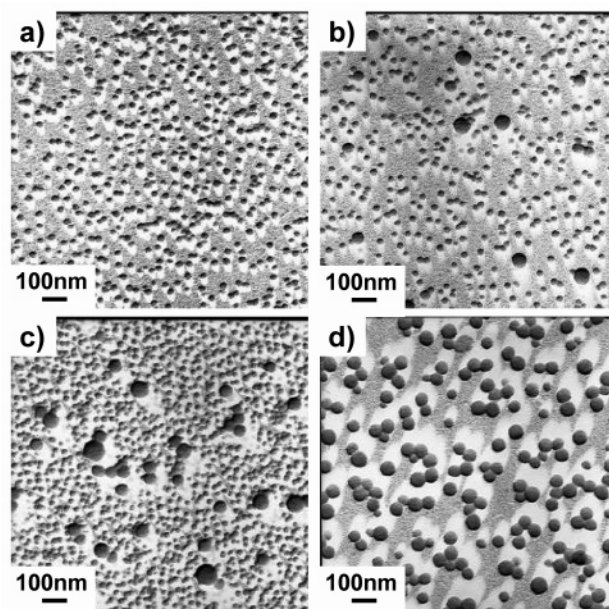


Figure 2. Effect of blend composition, f , on self-assembly of blends of PS300–CdS and PS(665)-*b*-PAA(68) in DMF/water. For all blends, $C_0 = 0.5$ wt % and $\text{rate}_{\text{H}_2\text{O}} = 1.2$ wt %/min. TEM images with Pt/Pd shadowing of dialyzed colloids obtained from the following compositions: (a) $f = 0$, (b) $f = 0.10$, (c) $f = 0.30$, and (d) $f = 0.50$.

Effect of PS300–CdS/PS(665)-*b*-PAA(68) Blend Composition on QDCM Formation. Before investigating QDCM size control, we first determined the blend composition that gave a single population of well-dispersed QDCM particles by secondary self-assembly. In the original paper on QDCM formation, it was shown that above a certain quantity of stabilizing chains, two coexisting particle populations were observed following water addition: QDCMs and crew-cut micelles containing no QDs. On the other hand, an insufficient quantity of stabilizing chains resulted in macroscopic precipitation or a bimodal QDCM population.³⁰

To determine the effect of the relative amount of stabilizing chains on QDCM formation, we prepared a series of blend solutions in DMF with constant total initial polymer concentration $C_0 = 0.5$ wt % and various weight fractions of PS300–CdS in the blends: $f = 0, 0.10, 0.30$, and 0.50 . (We note that, for similar blends using the same stabilizing chains, $f = 0.70$ and 0.90 compositions were found to result in precipitation rather than stable colloid formation upon water addition, so these compositions were not further investigated in this study.) To these four solutions was added water dropwise at a rate of $20 \mu\text{L}/20 \text{ s}$ ($\text{rate}_{\text{H}_2\text{O}} = 1.2$ wt %/min). For each clear yellow blend solution, the appearance of turbidity with water addition indicated the onset of self-assembly. Water was then continuously added at the same rate to a total water content of 25 wt %, followed by dialysis for 5 days against pure water to remove all remaining DMF. All four blend compositions resulted in stable aqueous colloids which were characterized by TEM.

TEM images of the self-assembled blend solutions $f = 0, 0.10, 0.30$, and 0.50 , deposited from aqueous colloids onto carbon/Formvar substrates and then shadowed with Pt/Pd, are shown in Figure 2. The Pt/Pd shadowing assists in increasing the contrast between the particles and the substrate and results in the teardrop-shaped shadow oriented along the direction of sputtering. TEM for the $f = 0$ sample (Figure 2a), which contained only PS-(665)-*b*-PAA(68) chains and no PS300–CdS, shows a single population of small spherical particles with average diameter

(52) Termonia, Y. *Macromolecules* **1997**, *30*, 5367.

(53) Byrne, A.; Timoshenko, E. G.; Dawson, K. A. *Physica A* **1997**, *243*, 14.

(54) Liu, H.; Bhattacharya, A.; Chakrabarti, A. *J. Chem. Phys.* **1999**, *111*, 11183.

~ 25 nm, which must be crew-cut micelles formed from self-assembly of the block copolymer alone. For the $f = 0.10$ sample (Figure 2b), we find a population of small particles similar to those observed in the $f = 0$ sample, along with a small number of larger spheres with average diameter ~ 50 nm. For $f = 0.30$ (Figure 2c), the same two particle populations are present, although the relative number of larger spheres has increased. Finally, for the $f = 0.50$ sample (Figure 2d), only the larger particles are present, with an average diameter $d_c = 52$ nm and a standard deviation of 9 nm.

TEM of the various blend compositions without Pt/Pd shadowing (Figure 3) allowed the internal structures of the various aggregates to be imaged, so the nature of the different particle populations could be assessed. For the $f = 0.10$ and $f = 0.30$ samples (parts a and b, respectively, of Figure 3), the smaller spheres appear as homogeneous circles without internal structure, while the larger spheres clearly show a distribution of electron-dense spots, attributed to CdS QDs, throughout the spherical polymer matrix. Unshadowed images of the particles obtained for $f = 0.50$ (Figure 3c) indicate that they also possess internal structure, similar to the larger particles in Figure 3a,b. The internal structure of these larger spheres observed in the $f = 0.10$, 0.30, and 0.50 blends is consistent with QDCMs, assemblies of block copolymer stabilizing chains and PS300–CdS illustrated in Scheme 2. The homogeneous nature of the smaller spheres observed in the $f = 0.10$ and $f = 0.30$ samples, and their similarity in size to the particles observed when no PS300–CdS is present ($f = 0$), confirms that they are crew-cut micelles arising from the self-assembly of PS(665)-*b*-PAA(68) stabilizing chains alone. Therefore, there appears to be an excess of stabilizing chains in the $f = 0.10$ and $f = 0.30$ blends as the QDCMs are formed, resulting in the formation of a separate crew-cut micelle population from residual PS(665)-*b*-PAA(68) as water is added above the CWC. However, a single population of only QDCMs, without crew-cut micelle formation, was obtained when the relative amount of PS300–CdS was increased to $f = 0.50$.⁵⁵ Having identified $f = 0.50$ as the optimum blend composition for the formation of a single QDCM population in the present system, this composition was used for all of the studies described in the following sections, as either the initial polymer concentration, C_0 , or the rate of water addition, $\text{rate}_{\text{H}_2\text{O}}$, is varied.

Kinetic QDCM Size Control via Initial Polymer Concentration. As mentioned previously, QDCM sizes will be governed by the window of growth between phase separation at the CWC and QDCM freezing at 8–11 wt % water. This provides a strategy for tuning the mean QDCM size via the initial polymer concentration. On the basis of studies of various PS homopolymers and PS-*b*-PAA block copolymers, Zhang et al. have shown that, for the same polymer, higher polymer concentrations result in lower CWCs.⁴⁸ This means that increasing the initial polymer concentration should lead to an earlier onset of QDCM formation as water is added at a given rate and consequently to a wider window for QDCM growth.

For the series of QDCM preparations described in this section, we used a constant blend composition, $f = 0.50$, and five different initial polymer concentrations: $C_0 = 0.5, 1.0, 2.0, 3.0,$ and 4.0 wt %. To induce self-assembly, water addition was carried out at a constant rate of $20 \mu\text{L}/20 \text{ s}$ ($\text{rate}_{\text{H}_2\text{O}} = 1.2 \text{ wt \%}/\text{min}$) up to

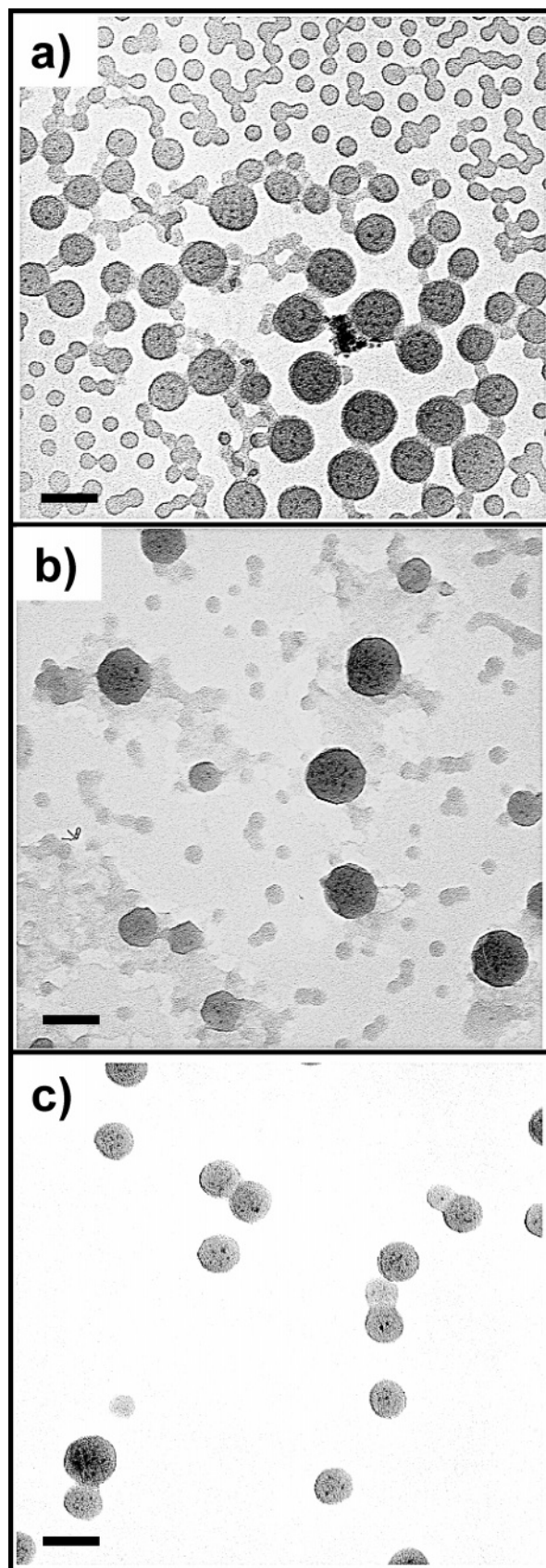


Figure 3. TEM images without Pt/Pd shadowing of the following colloids from Figure 2: (a) $f = 0.10$, (b) $f = 0.30$, (c) $f = 0.50$. For all blends, $C_0 = 0.5$ wt % and $\text{rate}_{\text{H}_2\text{O}} = 1.2$ wt %/min. The larger particles are QDCMs showing internal structure of dispersed CdS QDs. The scale bars represent 50 nm.

25 wt % water, and the CWC was noted for each initial polymer concentration by an increase in turbidity. The following CWCs,

(55) The blend composition at which a single, stable QDCM colloid is obtained without crew-cut micelle formation ($f = 0.50$) is notably different from that found in ref 30 ($f = 0.88$). This is explained by the different stabilizing chains used in that case, PS(1100)-*b*-PAA(170), which will form micelles at a lower water content than the stabilizing chains used in the present work, due to a longer PS block. Therefore, a larger percentage of stabilizing chains were added in the present study without crew-cut micelle formation.

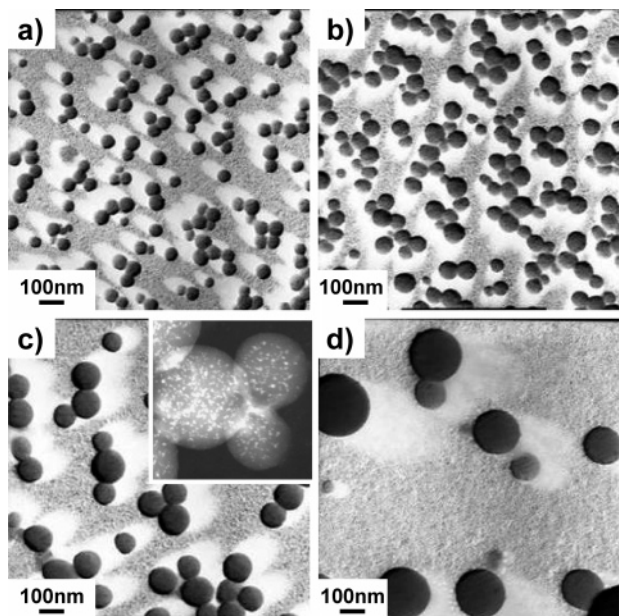


Figure 4. Effect of initial polymer concentration, C_0 , on self-assembly of blends of PS300–CdS and PS(665)-*b*-PAA(68) in DMF/water. For all blends, $f = 0.50$ and $\text{rate}_{\text{H}_2\text{O}} = 1.2$ wt %/min. TEM images with Pt/Pd shadowing of dialyzed QDCMs obtained from the following initial polymer concentrations: (a) $C_0 = 0.5$ wt %, (b) $C_0 = 1.0$ wt %, (c) $C_0 = 2.0$ wt %, (d) $C_0 = 3.0$ wt %. The inset to (c) (200×200 nm) shows a representative dark field image of internal structure of QDCM particles without Pt/Pd shadowing, where internal bright dots are QDs.

indicating the onset of QDCM formation, were recorded as a function of initial polymer concentrations: $C_0 = 0.5$ wt %, CWC = 2.3 wt %; $C_0 = 1.0$ wt %, CWC = 2.0 wt %; $C_0 = 2.0$ wt %, CWC = 1.6 wt %; $C_0 = 3.0$ wt %, CWC = 1.6 wt %; $C_0 = 4.0$ wt %, CWC = 1.2 wt %. These data confirm the expected decrease in the CWC with increasing initial polymer concentration, although they should be regarded as approximate values roughly determined from visual inspection of the solutions.

TEM images of QDCM samples prepared from different initial polymer concentrations, following dialysis and transfer to pure water, are shown in Figure 4. The $C_0 = 4.0$ wt % sample is not shown but will be discussed in the following text. For all initial concentrations, we confirmed that only QDCM particles were observed without the presence of crew-cut micelles, on the basis of the size of the particles ($d_c \geq 50$ nm) along with their internal structure observed by TEM of unshadowed particles. The internal structure of these spherical assemblies is demonstrated by the representative dark field STEM image (Figure 4c, inset), showing multiple bright QDs throughout particles formed from the $C_0 = 2.0$ wt % solutions. The shadowed TEM images reveal a progressive increase in QDCM particle size as the initial polymer concentration increases from 0.5 to 3.0 wt %. This tunable size increase is shown quantitatively by the size distribution analysis in Figure 5, obtained by measuring at least 325 particles randomly sampled from various regions of the grids for the four samples represented in Figure 4. From this distribution analysis, we find that the mean QDCM size progressively increases from $d_c = 50$ nm to $d_c = 209$ nm as the initial polymer concentration increases from $C_0 = 0.5$ wt % to $C_0 = 3.0$ wt %, while the standard deviation (SD) also increases, from SD = 18% to SD = 30%. The $C_0 = 4.0$ wt % sample was also characterized by TEM and was found to contain extremely large and polydisperse particles (diameters up to $2 \mu\text{m}$) which were agglomerated on the TEM grid and therefore impossible to characterize by particle size analysis.

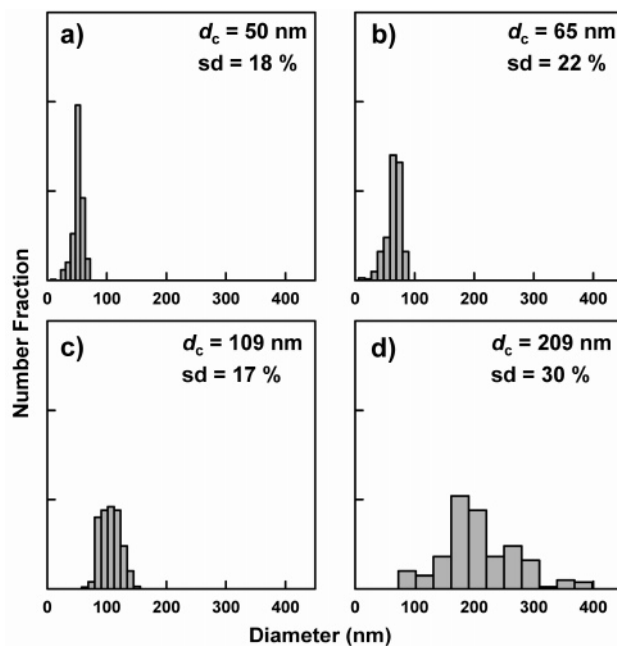


Figure 5. Distributions of QDCM core sizes from TEM data for different initial polymer concentrations ($f = 0.50$, $\text{rate}_{\text{H}_2\text{O}} = 1.2$ wt %/min): (a) $C_0 = 0.5$ wt %, (b) $C_0 = 1.0$ wt %, (c) $C_0 = 2.0$ wt %, (d) $C_0 = 3.0$ wt %. Mean sizes, d_c , and SDs are indicated for each distribution.

The increase in polydispersity with increasing particle size can be explained by the nonequilibrium nature of phase coarsening and suggests particle coalescence, rather than Ostwald ripening, as the predominant mechanism for QDCM growth. This highlights the kinetic nature of the current method of QDCM size control, by which particles are given more time to grow before freezing as the initial polymer concentration is increased, due to earlier CWCs afforded by higher polymer concentrations. Along with a wider temporal window for growth, an increased rate of phase separation and coarsening with increased polymer concentration may also contribute to the observed concentration dependence of QDCM size.⁵⁴ We note that size control at the expense of increased size polydispersity with increased average particle size is not ideal when low polydispersity and large particle sizes are both desired. We are currently seeking self-assembly conditions under which QDCM particle size distributions can be lowered over a broader range of sizes, along with exploring post-assembly methods of particle fractionation.

To test reproducibility, we carried out a repeat run of the QDCM preparations described above by preparing an identical series of initial blend concentrations from new stock solutions. The same rate of water addition and the same stir rate were applied in the repeat experiments. Particle size analysis from TEM images of the repeat series (not shown) showed good agreement between mean QDCM diameters for repeat runs of the same initial polymer concentration, with most concentrations giving $\leq 6\%$ difference between runs. The average diameters from the two repeat runs are plotted vs initial polymer concentration in Figure 6, with errors determined from the difference between repeat experiments. This plot highlights the demonstrated reproducible kinetic control of mean QDCM particle diameters in the range of ~ 50 – 200 nm, by variation of the initial polymer concentration from 0.5 to 3.0 wt % with all other experimental parameters held constant.

From QDCM sizes determined for different initial polymer concentrations, various important QDCM structural parameters were calculated. For these calculations, we consider that the

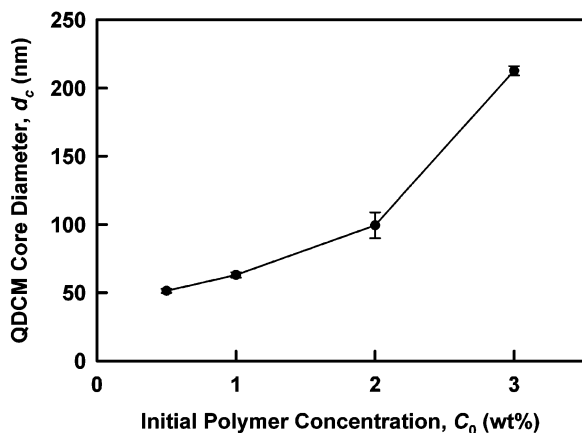


Figure 6. Mean QDCM core sizes, d_c ($f = 0.5$, $\text{rate}_{\text{H}_2\text{O}} = 1.2$ wt %/min), vs initial polymer concentration, C_0 . Errors are determined from repeat experiments under identical conditions. Lines connecting data points are shown as a guide for the eye.

QDCM diameters described above were determined by TEM from particles deposited onto a substrate and sputtered with Pd/Pd under vacuum. The diameter, d_c , therefore represents the mean size of the QDCM core region only (Scheme 2) and does not include the PAA layer: PAA chains will collapse onto the rigid QDCM core surface upon removal of water and will not contribute significantly to the particle dimensions observed by TEM. From QDCM core diameters obtained from different initial polymer concentrations (Figures 4 and 5), we first calculated the average number of PS300–CdS particles, $n_{\text{PS-CdS}}$, within each QDCM assembly. Since each PS300–CdS particle contains approximately one CdS QD,^{41,44} $n_{\text{PS-CdS}}$ is simply the number of QDs assembled within a QDCM. The value of $n_{\text{PS-CdS}}$ for each initial polymer concentration was determined by first calculating the average volume of the QDCM core, $V_c = 4/3\pi r_c^3$, where $r_c = d_c/2$ is the QDCM core radius; the mass of the core was then determined assuming a density of ~ 1 g/mL (close to the bulk density of PS). From the core mass, the number of PS300–CdS particles making up each QDCM can finally be calculated using the blend composition $f = 0.50$ assuming a statistical distribution of stabilizing chains throughout the sample. Values of $n_{\text{PS-CdS}}$ determined for the various initial polymer concentrations are listed in Table 2, demonstrating a tunable increase in the number of QDs per assembly from 12 to 840. We note that while the QDCM core diameter, d_c , increases by a factor of 4.2 as the initial polymer concentration is increased from 0.5 to 3.0 wt %, the number of QDs per assembly increases by a factor of 70; this follows from the d_c^3 scaling of $n_{\text{PS-CdS}}$, which is proportional to the QDCM core volume.

The assumptions of bulk PS core density and a statistical distribution of stabilizing chains were also used to calculate the surface density of PAA chains, σ_{PAA} , for each initial polymer concentration (Table 2). The average number of stabilizing chains per QDCM scales linearly with the core mass (which is proportional to V_c) and therefore scales as d_c^3 . The average surface area per QDCM is determined from $A_c = 4\pi r_c^2$ and thus scales as d_c^2 . Therefore, σ_{PAA} (PAA chains/nm²) scales linearly with d_c ; the linear relation between the calculated PAA surface densities, σ_{PAA} , and the measured QDCM particle sizes, d_c , is confirmed in Figure 7. As the QDCM particle sizes increase for a constant number of stabilizing chains per unit volume of polymer, the total surface area of the system decreases, resulting in more densely packed PAA at the polymer/solvent interface. As a result, the surface density of PAA chains in the external

QDCM stabilizing layer is tuned along with particle diameter via the initial polymer concentration.

Kinetic QDCM Size Control via Rate of Water Addition.

We now demonstrate another strategy for kinetic QDCM size control by varying the rate of dropwise water addition, $\text{rate}_{\text{H}_2\text{O}}$. For this series of experiments, both the blend composition and initial polymer concentration were held constant at $f = 0.50$ and $C_0 = 0.5$ wt %, respectively. The initial blend solutions in DMF were therefore identical for the five experiments in this series, with the rate of water addition during QDCM formation being the only experimental variable: $\text{rate}_{\text{H}_2\text{O}} = 4.8, 2.4, 1.2, 0.6,$ or 0.4 wt %/min.

TEM images of these experiments following dialysis were again obtained, with each sample showing a single distribution of QDCM particles, with d_c increasing from 45 to 57 nm as the rate of water addition was decreased from 4.8 to 0.4 wt %/min. Size distribution widths did not vary significantly in this range of sizes, with standard deviations falling in the range of 17–20% for all QDCM samples. Reproducibility was again tested with a repeat series of experiments under identical conditions: average d_c values from the two runs are plotted vs the rate of water addition in Figure 8, with errors determined from the difference between repeat runs. Though the scatter in this plot is greater than that obtained for QDCM size control as a function of initial polymer concentration, the trend of decreasing QDCM size with increasing rate of water addition is clear. As water is added at a faster rate, QDCM particles experience less growth time between the CWC and the water content at which freezing occurs, resulting in the kinetic trapping of smaller particles.

Dynamic Light Scattering Measurements and Determination of PAA Layer Thickness. As previously mentioned, QDCM diameters determined by TEM, d_c , represent only the QDCM cores (Scheme 2) and do not therefore reflect the external layer of PAA chains at the QDCM surface. However, the solubilized PAA layer is critical for the stability of the QDCM colloid against agglomeration and precipitation. As well, the thickness of this layer will significantly affect the size of QDCM particles in aqueous media and will therefore influence particle transport and interparticle interactions—two important issues for biological and photonic applications. It was therefore of interest to determine the hydrodynamic diameters of the QDCM particles dispersed in water, $d_{\text{h,QDCM}}$, which will include both the core and the solvated PAA brush layer.

For the series of QDCM samples with varying core sizes (Table 2), prepared from different initial polymer concentrations and previously analyzed by TEM, DLS measurements were carried out in pure deionized water, following dialysis and dilution to a single concentration in the range of 0.1–0.01 mg/mL (depending on the sample scattering intensity). Effective hydrodynamic radii were determined from cumulant analysis of the autocorrelation function at a scattering angle of 90°.

The $d_{\text{h,QDCM}}$ values reported in Table 2 are all larger than d_c values determined by TEM for the same sample, consistent with the presence of an external solubilized PAA layer in aqueous solution. As well, $d_{\text{h,QDCM}}$ is found to increase with C_0 , which is the same trend observed for the core size, d_c . By combining the two diameters $d_{\text{h,QDCM}}$ and d_c , determined from DLS and TEM, respectively,⁵¹ we are able to calculate the average thickness of the external PAA layer in solution, t_{PAA} (Table 2), using

$$t_{\text{PAA}} = (d_{\text{h,QDCM}}/2) - (d_c/2) \quad (1)$$

As shown in Scheme 2, the thickness of the PAA layer is related to the extension of tethered PAA blocks from the QDCM surface into solution. The pH of selected QDCM solutions

Table 2. Structural Characteristics of QDCMs in Water (pH 6) Prepared from Various Initial Polymer Concentrations (TEM and DLS Data)

C_0 (wt %)	d_c^a (nm)	n_{PS-CdS}	σ_{PAA} (chains/nm ²)	t_{max}/r_c	$d_{h,QDCM}^b$ (nm)	t_{PAA} (nm)	PAA extension (%)
0.5	50 ± 1	12 ± 1	0.035 ± 0.001	0.68 ± 0.13	68 ± 3	9 ± 2	50 ± 10
1.0	65 ± 2	25 ± 4	0.045 ± 0.004	0.52 ± 0.08	95 ± 4	15 ± 2	90 ± 10
2.0	109 ± 2	120 ± 10	0.076 ± 0.006	0.31 ± 0.06	143 ± 5	17 ± 3	100 ± 20
3.0	209 ± 10	840 ± 160	0.14 ± 0.02	0.16 ± 0.05	243 ± 9	17 ± 7	100 ± 40

^a Error on mean QDCM core diameters determined from error = $\pm(1.96(SD)/\sqrt{N})$; 1.96 is a constant for the 95% confidence level, SD is the standard deviation of the size distribution, and N is the number of particles measured from TEM images. ^b Error on z -average hydrodynamic diameters determined from the standard deviation of three repeat DLS measurements.

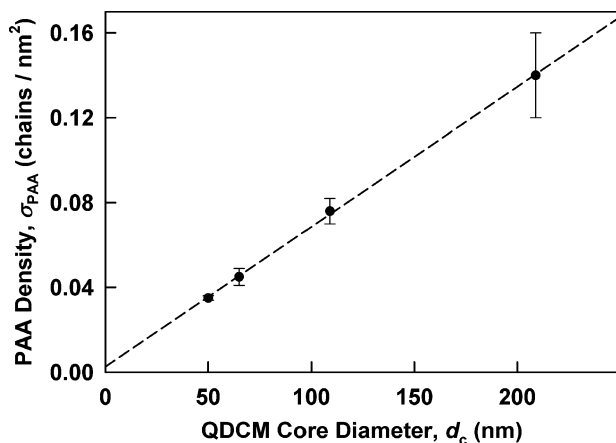


Figure 7. Surface density of PAA chains in a QDCM stabilizing layer, σ_{PAA} , vs mean QDCM core sizes, d_c . A linear relationship (linear regression shown) is expected from the scaling relations, as discussed in the text.

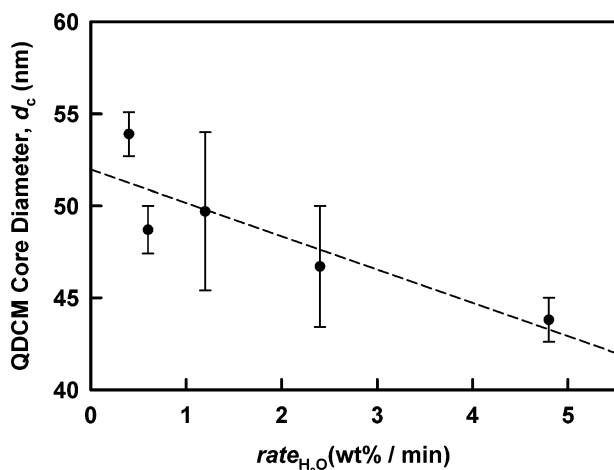


Figure 8. Mean QDCM core sizes, d_c ($f = 0.5$, $C_0 = 0.5$ wt %), vs rate of water addition, $rate_{H_2O}$. Errors are determined from repeat experiments under identical conditions. Linear regression is shown as a guide for the eye and is not meant to represent the best fit of data points.

following dialysis against deionized water was measured and found to be 6 for different particle sizes. In aqueous media at $pH > 4$, linear PAA is partially ionized, with the degree of ionization increasing with pH .^{51,56} Therefore, the PAA chains on the QDCM surface are expected to be negatively charged, such that the PAA layer represents a colloidal polyelectrolyte brush.^{51,56–60} In such systems, the stretching of chains relative to their random coil dimensions, and therefore the brush thickness,

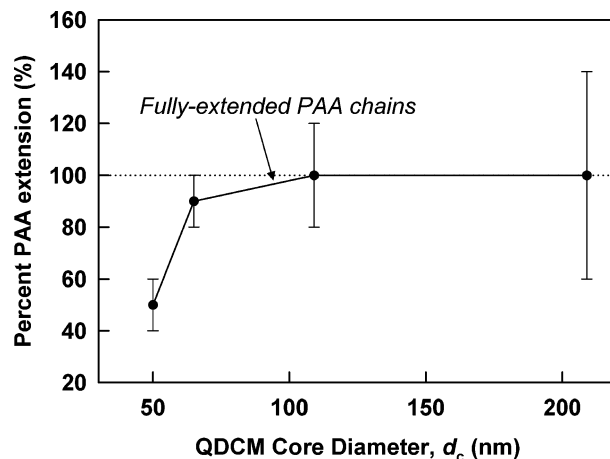


Figure 9. Extension of PAA chains in a QDCM stabilizing layer (%) (from combined TEM and DLS data) vs mean QDCM core sizes, d_c . The dotted line indicates the fully extended PAA chain conformation.

will be dependent on a combination of steric and electrostatic repulsion between the tethered chains.

The PAA brush thickness is equal to the average end-to-end distance of PAA chains within the brush, such that the percent PAA chain extension relative to full chain extension can be calculated from t_{PAA} using the following formula:

$$\text{PAA extension (\%)} = 100(t_{PAA}/[aN_{PAA}]) \quad (2)$$

where N_{PAA} is the number of acrylic acid repeat units in the chains ($N_{PAA} = 68$) and a is the length of one fully extended acrylic acid repeat unit ($a = 0.25$ nm).⁵¹ The resulting values range from 50% to 100% chain extension for different QDCM sizes (Table 2). A plot of PAA chain extension vs the QDCM core diameter, d_c (Figure 9), shows that PAA stretching increases with d_c , reaching a fully extended conformation for sufficiently large particles. Very high extension of polyelectrolyte chains, like “porcupine quills”⁵⁷ radiating from the colloidal particle, has been predicted by theory for polyelectrolyte colloids in the absence of salt^{57–60} and has been previously observed in the coronae of PS-*b*-PAA crew-cut micelles.⁵¹ Fully extended PAA chains at the surface of QDCM particles at $pH 6$ in water are therefore a reasonable result, consistent with the presence of strong mutual repulsion between charged chains within colloidal brushes in a good solvent.

The observed increase in the extension of PAA chains on QDCMs with increasing particle size is an interesting result and indicates that the demonstrated kinetic control of the QDCM core diameter (Figures 6 and 8) allows the conformation of the

(56) Currie, E. P. K.; Sieval, A. B.; Fleer, G. J.; Cohen Stuart, M. A. *Langmuir* **2000**, *16*, 8324.

(57) Pincus, P. *Macromolecules* **1991**, *24*, 2912.

(58) Guo, X.; Ballauff, M. *Langmuir* **2000**, *16*, 8719.

(59) Hariharan, R.; Biver, C.; Mays, J.; Russel, W. B. *Macromolecules* **1998**, *31*, 7506.

(60) Biver, C.; Hariharan, R.; Mays, J.; Russel, W. B. *Macromolecules* **1997**, *30*, 1787.

PAA stabilizing layer to be tuned. To understand the observed relationship between QDCM core size and PAA chain stretching, we must first consider the various factors that influence chain conformation within a polyelectrolyte brush. The addition of added salt is known to increase the ionic strength within the brush, which can decrease chain stretching via Debye screening;^{51,57–59} however, since no salt has been added to any of our samples, and all QDCMs were dialyzed against deionized water, this screening effect is not believed to be significant here.

The surface density of chains, σ , is well-known to influence the thickness of polymer brushes.⁵¹ In neutral brushes, higher surface densities will generally increase chain stretching due to increased overlap between neighboring chains;⁶⁰ however, for polyelectrolyte brushes in the limit of zero salt concentration, the effect of chain density on the brush thickness is quite complex. Pincus has predicted the brush thickness to be independent of σ in this limit;⁵⁷ theoretical predictions for brushes of weak polyacids, including PAA, conclude that the chain stretching will decrease with increasing σ , due to the decrease in the degree of dissociation of acid groups with σ at constant pH.⁵⁶ On the other hand, various experimental results for polyelectrolyte brushes in the zero-salt limit have determined that brush thickness and therefore chain stretching increase with surface density, even for brushes of weak polyacids.^{56,58,59} In the present case, we have determined that σ_{PAA} increases with d_c due to a decrease in the total system surface area (Figure 7), which could contribute to the observed increase in the thickness of the PAA layer. Surface curvature is another important factor which influences the conformation of chains within polymer brushes on the surface of a colloidal particle.^{57–60} Surface curvature is generally expressed as the ratio of the maximum brush thickness, t_{max} , to the particle radius, r : t_{max}/r . As the curvature increases for constant surface density, segment–segment interactions are expected to decrease, resulting in decreased chain stretching relative to a flat surface, $r \gg t_{\text{max}}$. We have calculated the curvature parameter, t_{max}/r_c , for each of the QDCMs described in Table 2 ($r_c = d_c/2$ and $t_{\text{max}} = aN_{\text{PAA}} = 17$ nm), showing the curvature to decrease significantly as d_c increases from 50 nm ($r_c \approx t_{\text{max}}$) to 209 nm ($r_c \gg t_{\text{max}}$). From the above discussion, it therefore appears that a combination of increased σ_{PAA} and decreased curvature will contribute to the observed increase in PAA chain stretching with increasing QDCM particle size (Figure 9).

Photoluminescence of QDCMs. Applications in photonics and biolabeling require that the PL of individual dispersed QDs be maintained with secondary self-assembly into QDCMs. Figure 10 shows normalized and smoothed PL spectra of two of the QDCM samples described in Table 2 ($d_c = 109$ and $d_c = 209$), compared to the PL spectra of PS300–CdS dispersed in toluene. The PL spectra of the two QDCM samples are very similar, and both show good overlap with the PL spectrum of the constituent block copolymer-stabilized QDs prior to QDCM formation. This suggests that the QD size and surface environment are protected during self-assembly. We note that the band edge emission in both QDCM samples is somewhat suppressed relative to that of PS300–CdS and that the spectra appear to be slightly red-shifted for the QDCMs relative to the individual dispersed QDs. Some of these differences may be due to an increase in diffuse light scattering from the QDCM colloids, which appear turbid (even after dilution), compared to clear solutions of PS300–CdS in organic solvents. However, it is possible that interparticle dipole–dipole coupling within QDCMs may also contribute to the observed red shift, as discussed below.

The fact that the main PL features of individual QD building blocks are maintained upon self-assembly into QDCMs indicates

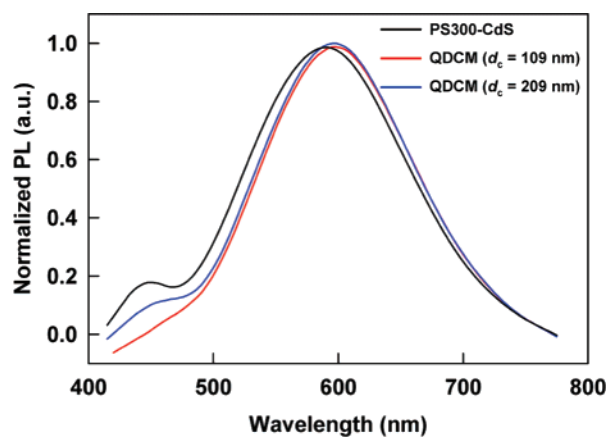


Figure 10. PL spectra of two QDCM samples ($d_c = 109$ nm, red curve; $d_c = 209$ nm, blue curve) in water compared to constituent PS300–CdS particles dispersed in toluene (black curve). For all spectra, $\lambda_{\text{ex}} = 400$ nm.

that the QDs are well protected from agglomeration, ripening, and surface changes within the stable block ionomer micelle of PS300–CdS, even as the PS corona is subjected to extreme changes in its environment (Scheme 3). In this sense the hydrophobic ionomer micelle acts as a “Trojan horse”, allowing QDs to be carried into colloidal assemblies of various sizes while maintaining a constant and protective local environment. This protective environment does not preclude through-space interactions between QDs within QDCM assemblies: energy transfer between QDs⁶¹ and surface plasmon–QD interactions between metal and semiconductor nanoparticles⁶² are possible if interparticle distances within the assemblies are on the order of 10 nm or lower. The distance between QDs within the assemblies can be tuned via the composition of the block copolymer used to template and stabilize the QDs and will be governed by the aggregation number and PS block length of the block copolymer-stabilized building blocks, independent of QDCM size. For all QDCMs in this study, we calculated that PS300–CdS gave an average interparticle spacing of ~ 12 nm within the assemblies (assuming bulk PS density and BCC arrangement of QDs), which should allow for some dipole–dipole coupling between neighboring QDs. The resulting transfer of energy from small to large QDs within the size distribution could therefore explain the slight red shift upon QDCM formation.

Conclusions

These results demonstrate excellent control of QD self-assembly within mesoscale hierarchical polymeric colloids (QDCMs). We show that the self-assembly process can be tuned via simple variation of experimental conditions which influence the time scale of particle growth. We have described two kinetic strategies for the size control of QDCMs, demonstrating that the QDCM core diameters, d_c , can be increased by increasing the initial polymer concentration or by decreasing the rate of water addition. As well, we have shown that the thickness of the external PAA layer, and consequently the PAA chain stretching, increases with increasing QDCM size, reaching the limit of fully extended chains for sufficiently large particles. This suggests strong electrostatic repulsion between charged stabilizing chains, which increases with higher chain surface density and lower curvature as d_c increases. In addition, the photoluminescence spectra from

(61) Murray, C. B.; Kagan, C. R.; Bawendi, M. G. *Annu. Rev. Mater. Sci.* **2000**, *30*, 545.

(62) Kulakovich, O.; Strekal, N.; Yaroshevich, A.; Maskevich, S.; Gaponeko, S.; Nabiev, I.; Woggon, U.; Artemyev, M. *Nano Lett.* **2002**, *2*, 1449.

QDCMs of different sizes in water were found to be nearly identical with the spectrum of constituent PS300–CdS particles dispersed in organic solvent, indicating that the size and surface environment of the QDs are well protected within micelle cores during QDCM formation. This level of control in the multiscale engineering of complex nanoparticle/polymer colloids should provide new avenues of tuning material properties for various applications in photonics and biolabeling.

Acknowledgment. We gratefully acknowledge the National Science and Engineering Research Council (NSERC), the Canadian Foundation for Innovation (CFI), and the British

Columbia Knowledge Development Fund (BCKDF) for their generous support of the research.

Supporting Information Available: Photoluminescence emission spectra of PS300–CdS in toluene for different excitation wavelengths, details of SLS and DLS measurements of PS300–CdS in DMF, details of calculation of $n_{\text{PS-CdS}}$, the number of QDs per QDCM, from the QDCM core diameter, d_c , and details of calculation of the PAA surface density, σ_{PAA} , from the QDCM core diameter, d_c . This information is available free of charge via the Internet at <http://pubs.acs.org>.

LA0623634